Plasma Chem Plasma Process (2013) 33:1167–1178
DOI 10.1007/s11090-013-9478-0

ORIGINAL PAPER

Laser Based Optical Emission Studies of Zinc Oxide (ZnO) Plasma

M. Hanif · M. Salik · M. A. Baig

Received: 12 May 2013 / Accepted: 9 August 2013 / Published online: 23 August 2013

Abstract We present the optical emission characteristics of the zinc oxide (ZnO) plasma produced by the first (1,064 nm) and second (532 nm) harmonics of a Q switched Nd: YAG laser. The target material was placed in front of laser beam in air (at atmospheric pressure).The experimentally observed line profiles of neutral zinc (Zn I) have been used to extract the electron temperature using the Boltzmann plot method, whereas, the electron number density has been determined from the Stark broadening. The electron temperature is calculated by varying distance from the target surface along the line of propagation of plasma plume and also by varying the laser irradiance. Beside we have studied the variation of number density as a function of laser irradiance as well as its variation with distance from the target surface. It is observed that electron temperature and electron number density increases as laser energy is increased.

Keywords Zinc oxide plasma · Laser ablation · Optical emission spectroscopy · Electron temperature · Electron number density

Introduction

Laser-induced breakdown spectroscopy (LIBS), also known as laser-induced plasma spectroscopy (LIPS) has developed rapidly as an analytical technique over the past few decades [1]. It employs a low-energy pulsed laser (typically tens to hundreds of mJ per pulse) and a focusing

M. Hanif (✉)
MCS, National University of Sciences & Technology, Rawalpindi, Pakistan
e-mail: hanif_muhammad@yahoo.com; drhanif-mcs@nust.edu.pk

M. Salik
Institute of Optoelectronics, Beijing Jiaotong University, Beijing, China

M. A. Baig
National Center for Physics, Quaid-E-Azam University Campus, Islamabad, Pakistan

lens, to generate plasma on the surface of a target. The spectrum of the plasma plume is the signature of the chemical species in the sample and its analysis yields their composition and relative abundance [2]. LIBS technique is unique that can be used to chemically analyze rocks, glasses, metals, sand, teeth, bones, powders, hazardous materials, liquids, plant, biological material, polymers, and ceramics etc [3]. The laser-produced plasma characteristics depend on several parameters including target features (physical and chemical properties), ambient medium properties (chemical composition and pressure), and laser pulse properties (pulse width, wavelength, spot size, and laser energy) [4]. Cao et al. [5] observed large second-order nonlinear optical response from zinc oxide (ZnO) thin films deposited on sapphire substrates by pulsed laser ablation. Sheikh et al. [6] reported spectroscopic studies of the zinc plasma produced in air by the three harmonics of a Q-switched pulsed Nd: YAG laser at 1,064, 532 and 355 nm. Saji et al. [7] reported optical emission spectroscopic studies of the plasma produced by ablation of ZnO target using the third harmonic (355 nm) of *Q*-switched Nd: YAG laser, in vacuum and at three different ambient gas (oxygen) pressures. Sheikh et al. [8] reported the measurement of the zinc and cadmium plasma parameters produced by the fundamental, second, and third harmonics of the Nd: YAG laser. Vestin et al. [9] used LIBS technique for investigation of chemical analysis in the single-shot regime for low-alloyed zinc samples. Shpenik et al. [10] reported post-collision interaction upon electron excitation of $4sns\ ^1S_0$, $^3S_1$ and $4snd\ ^1D_2$, ^3D_J levels of zinc atom. de Posada et al. [11] presented self-absorption influence on the optical spectroscopy of ZnO laser produced plasma.

In the present work we have employed LIBS technique for the optical emission study of the ZnO plasma generated by the fundamental (1,064 nm) and second (532 nm) harmonics of a Nd: YAG laser. We report the spatial evolution of the ZnO plasma in which, experimentally observed line profiles of neutral zinc (Zn I) have been used to extract the electron temperature (T_e) using the Boltzmann plot method. Whereas, the electron number density (N_e) has been determined from the Stark broadening parameter. Beside we have studied the variation of electron temperature and electron number density as a function of laser energy.

The Sample

The sample under this study is Zinc Oxide Powder (Sigma-aldrich). A small amount of it was used to prepare a pallet of 13 mm diameter and 3 mm thickness with the help of hydraulic press machine. The powder was pressed by a load of 10 Ton for time duration of 5 min. The Scanning Electron Microscope (SEM) photograph of the ZnO is shown in Fig. 1. The mass % of the Zinc in the sample was 80.34.

The Experimental Setup

The experimental setup is shown in Fig. 2, and is same as that described in our previous work [12]. Briefly we used a Q-switched Nd: YAG (Quantel Brilliant) pulsed laser having pulse duration of 5 ns and 10 Hz repetition rate which is capable of delivering 400 mJ at 1,064 nm, and 200 mJ at 532 nm respectively. The laser pulse energy was varied by the flash lamp Q-switch delay through the laser controller, and the pulse energy was measured by a Joule meter (Nova-Quantel 01507). The laser beam was focused on the target using convex lens of 20 cm focal length. The ZnO sample was mounted on a three dimensional sample stage, which was rotated to avoid the non-uniform pitting of the target. The distance between the focusing

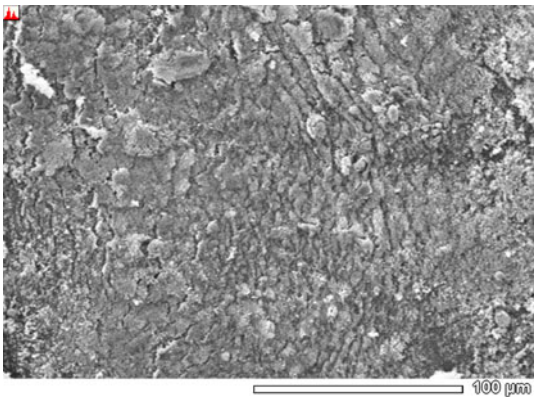

Fig. 1 SEM photograph of Zinc sample showing its morphology at 100 µm

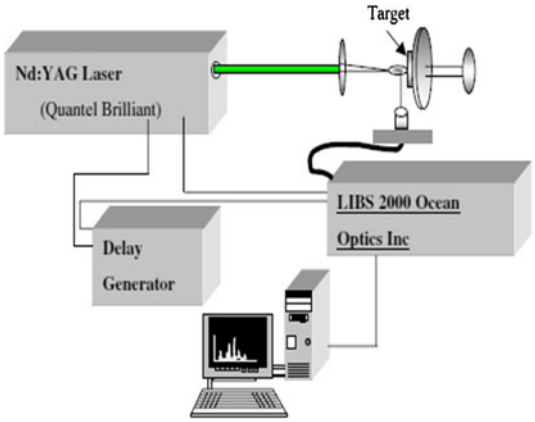

Fig. 2 Block diagram of the experimental setup

lens and the sample was kept less than the focal length of the lens to prevent any breakdown of the ambient air in front of the target. The diameter ω_2 of the spot size can be calculated using the relation $\omega_2 \approx 2.44f\lambda/\omega_1$ [3], where, ω_1 = diameter of the incoming laser beam before focusing (in our case its value is 0.5 cm), from where, one can calculate the area/size of the spot on the surface of the target, f is the focal length of the lens (in our case its value is 20 cm) and λ is the wave length of the laser used. In our case we have used fundamental (1,064 nm) and second (532 nm) harmonics of a Nd: YAG laser. Therefore, the area of spot size for the first harmonic (1,064 nm) and second (532 nm) are 8.4×10^{-5} cm^2 and 2.12×10^{-5} cm^2 respectively. The spectra were obtained by averaging 10 data of single shot under identical experimental conditions. The radiation emitted by the plasma were collected by a fiber optics (high-OH, core diameter: 600 µm) having a collimating lens (0–45^o field of view) placed at right angle to the direction of the laser beam. The optical fiber was connected with the LIBS-2000 detection system (Ocean Optics Inc.), to measure the plasma emission. The emission signal was corrected by subtracting the dark signal of the detector through the LIBS software. The LIBS-2000 detection system is equipped with five spectrometers each having slit width of 5 µm, covering the range between 200 and 720 nm. Each spectrometer has 2,048 element linear CCD array and an optical resolution of $\approx$0.05 nm by scanning a narrow bandwidth dye laser. In the experiments, the time delay between the laser pulses and the start of the data acquisition is about 3.5 µs, whereas the integration time is about 2.1 ms. In order to record the

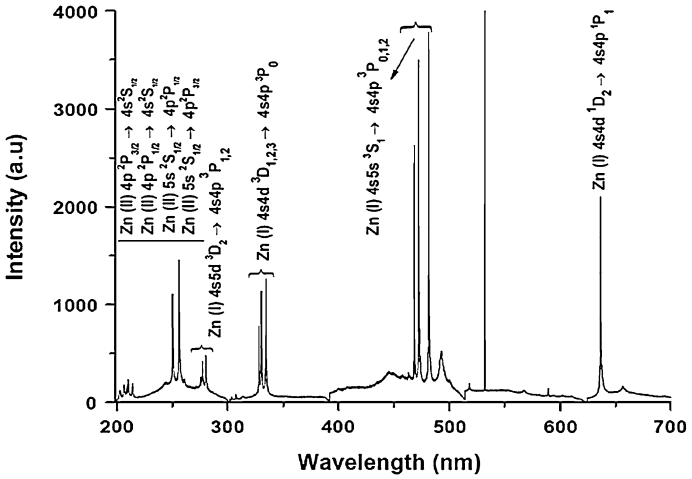

Fig. 3 The emission spectrum of ZnO plasma produced by fundamental (1,064 nm) harmonic of the Nd: YAG laser

emission spectrum, the LIBS-2000 detection system was synchronized with the Q-switch of the Nd: YAG laser. The flash lamp out of the Nd: YAG laser triggered detection system through a four-channel digital delay/Pulse generator (SRS DG 535).The LIBS-2000 detection system triggered the Q-switch of the Nd: YAG laser.

Results and Discussion

Emission Studies

In the first set of experiments, we have recorded the plasma produced by the fundamental (1,064 nm) and second (532 nm) harmonics of an Nd: YAG laser. The laser was focused by a quartz lens with a focal length of 20 cm. ZnO plasma was recorded at different positions along the direction of propagation of the plasma. Figure 3 shows the emission spectrum recorded at 532 nm laser, covering the spectral region from 200 to 720 nm. Both neutral as well as singly ionized zinc lines are present in this region. Figure 4 shows the emission spectrum recorded at 1,064 nm laser covering the spectral region from 325 to 485 nm. This portion of the spectrum predominantly shows the spectral lines of singly ionized zinc (Zn I) lines. The zinc spectral line at 328.23 nm corresponds to $4s4d\ ^3D_1 \rightarrow 4s4p\ ^3P_1$ transition, 468.01 nm to $5s\ 4s5s\ ^3S_1 \rightarrow 4s4p\ ^3P_0$, and 472.21 nm to $4s5s\ ^3S_1 \rightarrow 4s4p\ ^3P_1$ respectively. The strong resonance zinc line has been observed at 481.05 nm corresponding to $4s5s\ ^3S_1 \rightarrow 4s4p\ ^3P_2$ transition. The assignment of these spectral lines is straightforward as the levels belonging to the lower and upper state configurations are well known and are tabulated in the NBS (NIST) database [13].

Determination of Electron Temperature

Having observed the well-resolved multiplet structure from a number of excited levels and decaying to a common lower level, it is tempting to extract the plasma parameters from the observed spectra; in particular, the electron density and the plasma temperature. The spatial

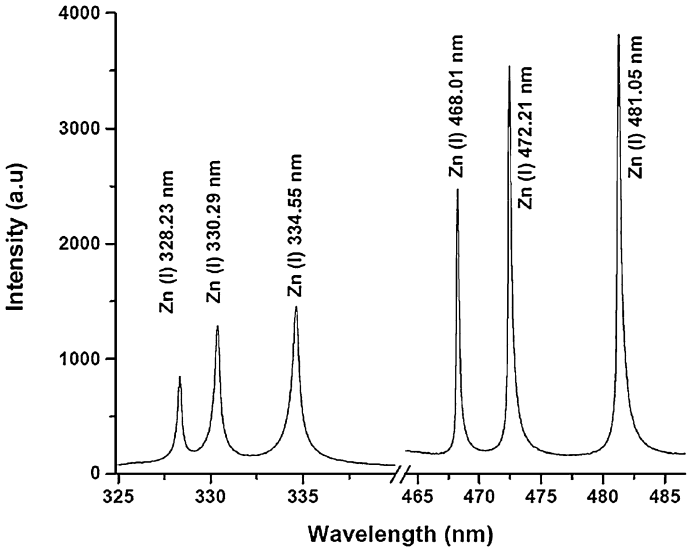

Fig. 4 The window spectra of ZnO plasma that used for the determination of electron temperature produced by fundamental (1,064 nm) harmonic of the Nd: YAG laser

behavior of the line intensities have been recorded using the fundamental (1,064 nm) and second (532 nm) harmonics of the Nd: YAG laser by varying the distance of the detector from the target surface along the plasma plume expansion. The plasma temperature is determined using the Boltzmann plot method from the relative intensities of the observed line; the relative intensities are normally proportional to the population of the pertinent upper levels. The following relation has been used to extract the plasma temperature [14]:

$$\ln\left(\frac{I_{ki}\,\lambda_{ki}}{A_{ki}g_k}\right) = \ln\left(\frac{N(T)}{U(T)}\right) - \frac{E_k}{kT} \tag{1}$$

where, I_{ki} is the integrated line intensity of the transition involving an upper level (k) and a lower level (i), λ_{ki} is the transition wavelength, A_{ki} is the transition probability, g_k is the statistical weight of level (k), $N(t)$ is the total number density, $U(T)$ is the partition function, E_k is the energy of the upper level, K is the Boltzmann constant and T is the excitation temperature. A plot of ln ($\lambda I/gA$) versus the term energy E_K gives a straight line with a slope equal to ($-1/KT$). Thus the plasma temperature can be determined without the knowledge of the total number density or the partition function. A typical Boltzmann plot is shown in Fig. 5. The line identifications and different spectroscopic parameters such as wavelength (λ_{ki}), statistical weight (g_k), transition probability (A_{ki}) and term energy (E_k) are listed in Table 1. For the determination of electron temperature of the plasma we have used the four neutral zinc (Zn I) lines at 328.23, 468.01, 472.21 and 481.05 nm respectively. Errors are bound to be present in the determination of the plasma temperature by this method therefore; the temperature is determined with $\pm$200 K uncertainty, coming mainly from the transition probabilities and the measurement of the integrated intensities of the spectral lines. The electron temperature of the plasma generated by the fundamental (1,064 nm) harmonic of the laser close to the target surface (at a distance of 0.05 mm) is estimated as 6,970 K that varies to 6,285 K at a distance of 2 mm from the target surface. The same experiment was repeated using

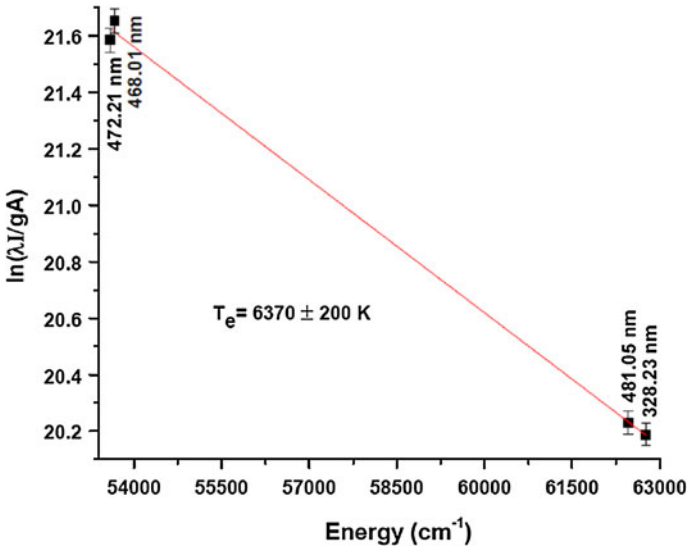

Fig. 5 Boltzmann plot based on four neutral zinc (Zn I) spectral lines using fundamental (1,064 nm) harmonic of the Nd: YAG laser

Table 1 Spectroscopic parameters of the observed neutral zinc (Zn I) lines

Wavelength λ (nm)	Transitions	Statistical weight (g_k)	Transition probability A (s^{-1})	Excitation energy E (cm^{-1})
328.23	$4s4d\ ^3D_1 \rightarrow 4s4p\ ^3P_1$	3	9.00×10^7	62,768.747
330.29	$4s4d\ ^3D_1 \rightarrow 4s4p\ ^3P_2$	3	6.70×10^7	62,768.747
334.55	$4s4d\ ^3D_2 \rightarrow 4s4p\ ^3P_2$	5	4.00×10^7	62,772.014
468.01	$4s5s\ ^3S_1 \rightarrow 4s4p\ ^3P_0$	3	1.55×10^7	53,672.24
472.21	$4s5s\ ^3S_1 \rightarrow 4s4p\ ^3P_1$	3	4.58×10^7	53,672.24
481.05	$4s5s\ ^3S_1 \rightarrow 4s4p\ ^3P_2$	3	7.00×10^7	53,672.24
636.23	$4s\ 4d\ ^1D_2 \rightarrow 4s4p^1P_1$	5	4.65×10^7	62,458.51

second (532 nm) harmonic of the laser, where the electron temperature varies from 6,815 to 6,175 K respectively over the same distance from the target surface. The variation in the electron temperature as a function of distance from the target surface for the plasma produced by the fundamental (1,064 nm) and second (532 nm) harmonics of Nd: YAG laser is shown in Fig. 6. The region near the target surface (at a distance of 0.05 mm) of the target material constantly absorbs radiation during the time interval of the laser pulse, causing a higher temperature near the target.

Determination of Electron Number Density

One of the most reliable techniques to determine the electron number density (N_e) is from the measured Stark broadened line profile of an isolated line of either neutral atom or single charge ion. The full-width at half maximum (FWHM) of the Stark broadening profile is related with the number density through the following relation [2, 3, 14]:

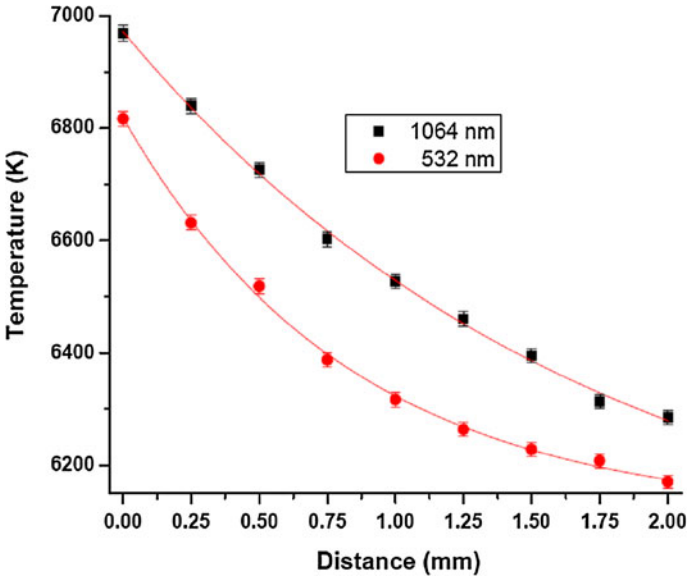

Fig. 6 Variation of the electron temperature along the direction of propagation of the plasma plume using fundamental (1,064 nm) and second (532 nm) harmonics of the Nd:YAG laser. The data points include 5 % *error bars* just to monitor the behaviour of electron temperature versus distance along the direction of propagation of plasma plume, whereas the *solid line* is a hand drawn *curve* which passes through all the data points

$$\Delta\lambda_{1/2} = 2\omega\left(\frac{N_e}{10^{16}}\right) + 3.5A\left(\frac{N_e}{10^{16}}\right)^{1/4}\left[1 - \frac{3}{4}N_D^{-1/3}\right]\omega\left(\frac{N_e}{10^{16}}\right) \tag{2}$$

where, ω is the electron impact width parameter, A is the ion broadening parameter, N_e is the electron number density and N_D is the number of particles in the Debye sphere. The first term in above Eq. (2) refers to the broadening due to the electron contribution, whereas, the second term is attributed to the ion broadening. Since the contribution of the ionic broadening is normally very small, therefore, it can be neglected. Therefore, Eq. (2) reduces to:

$$\Delta\lambda_{1/2} = 2\omega\left(\frac{N_e}{10^{16}}\right) \tag{3}$$

Here $\Delta\lambda_{1/2}$ is the width of the spectral line, ω is the electron impact broadening parameter and N_e is the electron number density. In Fig. 7, we show the line profile of the neutral zinc (Zn I) line at 481.05 nm along with the least squares fit of a Lorentzian line shape which yields the width $\Delta\lambda_{1/2}$ of this line. The Stark broadening parameter ω is available in the literature [14]. The condition that the atomic states should be populated and depopulated predominantly by electron collisions, rather than by radiation, requires an electron density which is sufficient to ensure the high collision rate. The corresponding lower limit of the electron density is given by the McWhirter criterion to check the condition for the validity of the local thermodynamic equilibrium (LTE) [15]:

$$N_e \geq 1.6 \times 10^{12}\ \mathrm{T}^{1/2}(\Delta E)^3 \tag{4}$$

where T(K) is the plasma temperature and $\Delta E(eV)$ is the energy difference between the states, which are expected to be in LTE. At ~6,970 K temperature, Eq. (4) yields

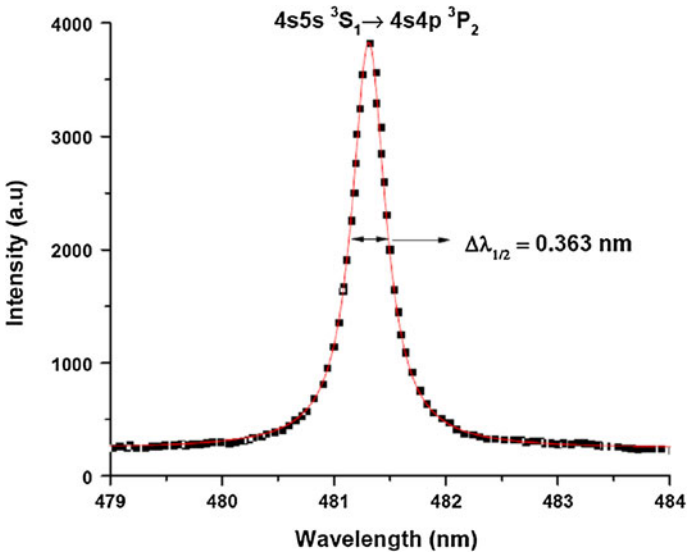

Fig. 7 Stark broadening profile of the neutral zinc line at 481.05 nm. The *dots* represent the experimental profile and the *solid line* is Lorentizian fit

$N_e \approx 10^{16}$ cm^{-3}. The electron number densities determined in our experiments are higher than this required number density to satisfy the LTE conditions. When the laser beam is focused on the target, the ablation of target takes place and due to the density gradient, the plasma rapidly expands.

Figure 8 shows the variation in the number densities using laser at 1,064 and 532 nm. The number densities close to the target surface (0.05 mm) are 2.88×10^{16} cm^{-3} and 3.02×10^{16} cm^{-3} and decrease to 1.74×10^{16} cm^{-3} and 1.80×10^{16}cm^{-3} at distances of 2 mm for 1,064 and 532 nm lasers respectively. The variation in the electron number density is very small for the 532 laser as compared with that of the 1,064 nm laser. The decrease in the number density at large distance is mainly due to the recombination of electrons and ions. The variation in the electron temperature is slower as compared with that of number density. The electron temperature and number density are different for the two wavelengths of the Nd: YAG laser, because of the difference in the energy per photon in each case. For any wavelength the incident energy is absorbed by the plasma as internal energy. The internal energy of the plasma is distributed in its thermal and ionization energy. It is a well known fact that the laser wavelength influences the ablation process. The electron number density is higher for the 532 nm laser than in the 1,064 nm laser. The particle density in the plasma depends on the degree of ionization, evaporation rate and the plasma expansion velocity. Because of the high expansion velocity of the leading plasma edge, the electron density decreases, makes the plasma transparent to the laser beam at larger distance away from the target surface. The absorption in the plasma mainly occurs by an inverse bremsstrahlung and photo ionization process.

Effect of Laser Irradiance

In the second set of experiments, we have determined the electron temperature and electron number density for different values of the laser irradiance by using Nd: YAG laser at

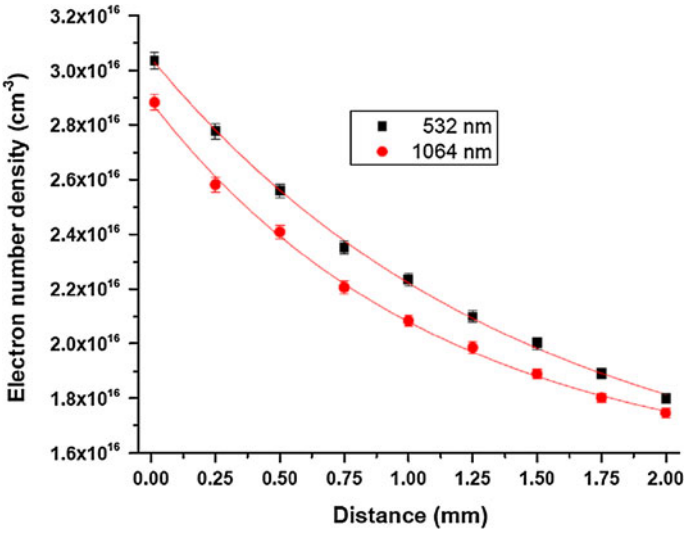

Fig. 8 Variation of the electron number density along the direction of propagation of the plasma plume using fundamental (1,064 nm) and second (532 nm) harmonics of Nd: YAG laser. The data points include 5 % *error bars* just to monitor the behaviour of electron number density versus distance along the direction of propagation of plasma plume, whereas the *solid line* is a hand drawn curve which passes through all the data points

1,064 nm and 532 nm wavelengths. We have observed that the intensities and widths of the spectral lines increase with the increase in the laser irradiance. Figure 9 shows the variation of the electron temperature for the laser produced ZnO plasma with respect to the laser irradiance at a distance of 0.05 mm from the target surface. In the case of 1,064 nm laser the electron temperature varies from 6,275 to 6,980 K, whereas, in the case of 532 nm laser the temperature varies from 6,029 to 6,855 K for the irradiance range from 2×10^{10} to 6.5×10^{10}W cm^{-2}. The figure shows that the electron temperature increases with the increase in the laser irradiance. Moreover with the increase in the laser irradiance the mass ablation rate also increases and hence the spectral line intensities and the widths increase as well. Figure 10 shows the variation of electron number density as a function of laser irradiance. The electron number density varies from 1.49×10^{16} to 3.06×10^{16} cm^{-3} for the 532 nm laser and it varies from 1.39×10^{16} to 2.92×10^{16} cm^{-3} in case of the 104 nm laser. The number density is slightly higher in the case of the 532 nm laser than that in the 1,064 nm laser. At higher laser energies, the increase in the plasma temperatures and electron densities increases very slowly this may be attributed to the plasma shielding. The two important mechanisms occurring in plasma are Inverse Bremsstrahlung (IB) and Photo-Ionization (PI). The IB process is usually described by the inverse absorption length which can be estimated from the relation [16]:

$$\alpha_{iB} \sim 1.37 \times 10^{-35} \lambda^3 N e^2 T_e^{-1/2} \tag{5}$$

here λ (μm) is the wavelength of the laser photons, T_e (K) is the electron temperature and N_e (cm^{-3}) is the electron density. In the case of 1,064 nm laser the IB absorption $\alpha_{i\beta}$ is $\approx$1.77 cm^{-1} at the laser irradiance of 5.5×10^{10} W cm^{-2}. The IB process is more efficient in the case of 1,064 nm laser as compared with the 532 nm laser because of its λ^3 dependence. Thus the number density in the case of 532 nm laser is higher than that of

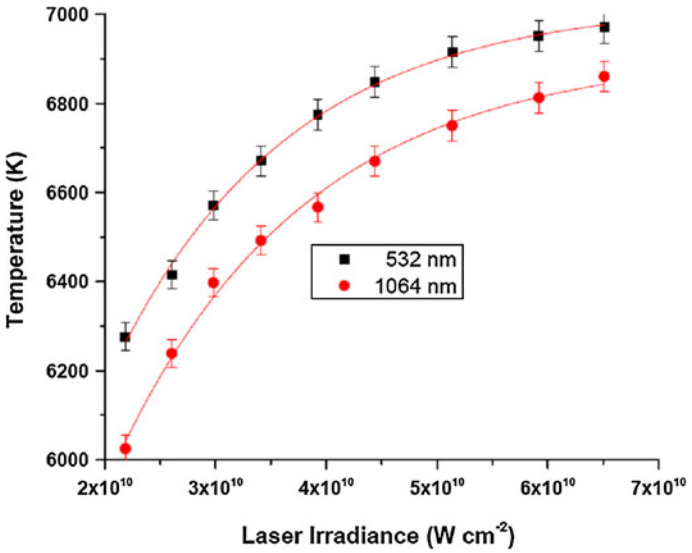

Fig. 9 Variation of the electron temperature with the laser irradiance using fundamental (1,064 nm) and second (532 nm) harmonics of the Nd: YAG laser. The data points include 5 % *error bars* just to monitor the behaviour of electron temperature vs laser irradiance, whereas the *solid line* is a hand drawn *curve* which passes through all the data points

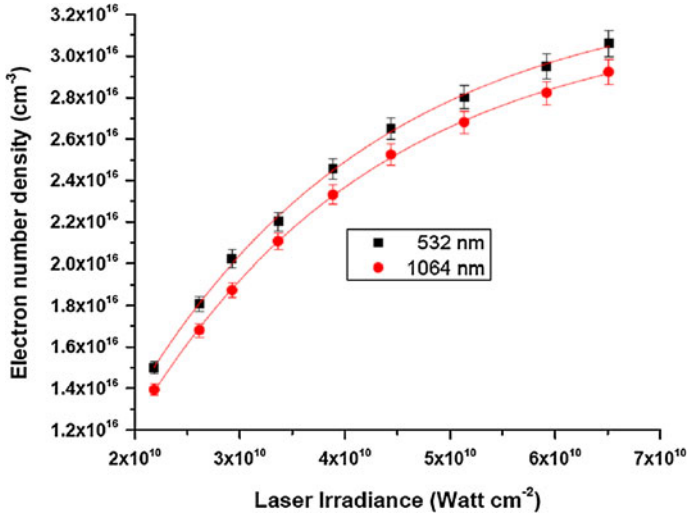

Fig. 10 Variation of the electron number density with the laser irradiance using fundamental (1,064 nm) and second (532 nm) harmonics of the Nd: YAG laser. The data points include 5 % *error bars* just to monitor the behaviour of electron number density vs laser irradiance, whereas the *solid line* is a hand drawn *curve* which passes through all the data points

1,064 nm laser, as is evident from Fig. 8 as well. We have also studied the energy behavior of the lines intensity for the Zn (I) prominent lines at 468.01, 472.21 and 481.05 nm originating from the $4s5s\ ^3S_1 \rightarrow 4s4p\ ^3P_0$, $4s5s\ ^3S_1 \rightarrow 4s4p\ ^3P_1$and $4s5s\ ^3S_1 \rightarrow 4s4p\ ^3P_2$

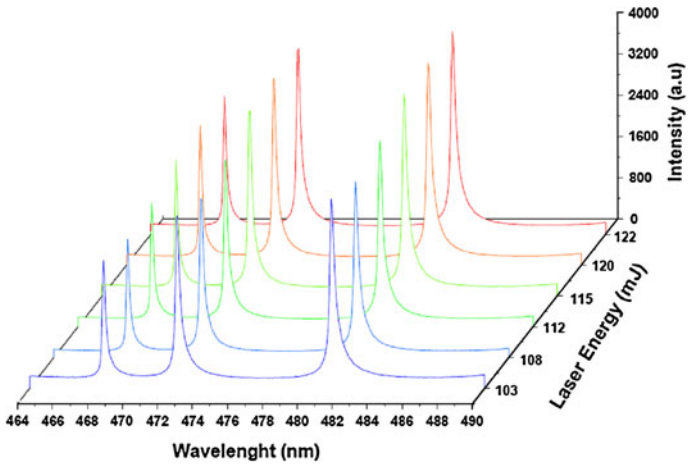

Fig. 11 Behavior of the spectrum of ZnO with variable energy along the direction of plasma plume using 1,064 nm laser at 0.05 mm distance from the target surface

transitions at the two laser wavelengths. Figure 11 shows the intensity behavior of these three lines of Zn (I) as the energy is varied from 96 up to 122 mJ in the case of 1,064 nm laser distance was adjusted at 0.05 mm. It is observed that the intensity of the line is much less when the spectrum is recorded at 103 mJ energy and it increase as we increased the laser energy up to 122 mJ. Identical trend has been observed at both the laser wavelengths. It is observed that the intensity of the line decreases by reducing the laser energy. The trend is similar for both the lasers. The higher laser energy produces greater ablation hence the intensities of the spectral lines are higher at higher laser energies.

Conclusion

The LIBS technique has been successfully applied as an analytical technique for the analysis of ZnO plasma using the fundamental (1,064 nm) and second (532 nm) harmonics of a Nd: YAG laser. The electron temperatures and number densities have been determined as a function of laser irradiance, laser wavelength and as a function of distance from the target surface along the plume expansion. It is observed that electron number density is higher for the 532 nm laser than that for the 1,064 nm laser, whereas the electron temperature is higher for the 1,064 nm laser higher than that for the 532 nm laser for the same value of laser irradiance and distance. The target material in the study [6] was pure zinc but experimental conditions were identical as in the present study, whereas, sample in the study [7] was same as in the present study but experimental conditions were different. Therefore, the present study is a good addition in the literature to understand the plasma parameters of the element of zinc in its pure as well as in oxide forms at atmospheric pressure.

References

1. Miziolek AW, Palleschi V, Schechter I (2008) Laser induced breakdown spectroscopy. Cambridge University Press, Cambridge

2. Cremers DA, Radziemski LJ (2006) Handbook of laser-induced breakdown spectroscopy. Wiley, New York
3. Singh JP, Thakur SN (2007) Laser-induced breakdown spectroscopy. Elsevier, Amsterdam
4. Chang JJ, Warner BE (1996) Appl Phys Lett 69(4):473–475
5. Cao H, Wu JY, Ong HC, Dai JY, Chang RPH (1998) Appl Phys Lett 73(5):572–574
6. Shaikh NM, Rashid B, Hafeez S, Jamil Y, Baig MA (2006) J Phys D Appl Phys 39:1384–1391
7. Saji KJ, Joshy NV, Jayaraj MK (2006) Appl Phys 100:043302 (5)
8. Shaikh NM, Hafeez S, Baig MA (2007) Spectro Acta Part B 62:1311–1320
9. Vestin F, Randelius M, Bengtson A (2010) Spectro Acta Part B 65:721–726
10. Shpenik OB, Erdevdi NM, Yu E (2011) Opt Spectrosc 110(3):351–362
11. de Posada E, Lunney JG, Arronte MA, Ponce L, Rodríguez E, Flores T (2011) J Phys Conf Ser 274:012079 (10)
12. Hanif M, Salik M, Sheikh NM, Baig MA (2012) Appl Phys B Lasers Opt 110(4):563–571
13. NIST, Hand book of basic atomic spectroscopic data: CD-ROM 23
14. Griem HR (1997) Principles of plasma spectroscopy. Cambridge University Press, Cambridge
15. McWhirter RWP (1965) Plasma diagnostic techniques. Academic Press, New York
16. Lou W, Sun Q, Gao C, Tang J, Wang H, Zhao W (2010) Plasma Sci Techno 12(4):385–390